A Compact *in situ* Polarized ^{3}He System for Neutron Scattering

Jian Tang[1,2,3,4†], Bin Wang[1,2,4,5†], Chuyi Huang[6], Han Gao[1,2,4], Qingbo Zheng[1,2,3,4], Renhong Liu[1,2,4], Fan Ye[1,2,4], Zecong Qin[1,2,4], Tianhao Wang[1,2,3,4], Ahmed Salman[1,2,4], Yuchen Dong[1,2,3,4], Long Tian[1,2,4], Changdong Deng[1,2], Jun Li[1,2], Lei Liu[1,2], Xin Qi[1,2,4], Junpei Zhang[1,2,3,4*], and Xin Tong[1,2,3,4*]

[1]*Institute of High Energy Physics, Chinese Academy of Science, Beijing 100049, China*
[2]*Spallation Neutron Source Science Center, Dongguan 523803, China*
[3]*University of Chinese Academy of Sciences, Beijing 100049, China*
[4]*Guangdong Provincial Key Laboratory of Extreme Conditions, Dongguan 523803, China*
[5]*Center for Neutron Science and Technology, Guangdong Provincial Key Laboratory of Magnetoelectric Physics and Devices, School of Physics, Sun Yat-Sen University, Guangzhou 510275, China*
[6]*Jülich Centre for Neutron Science at MLZ, Lichtenbergstr. 1, 85747 Garching, Germany*

(Received 15 October 2024; accepted manuscript online 13 January 2025)

This study investigates the performance of a new compact (55 cm × 56 cm × 48 cm) *in situ* spin-exchange optical pumping ^{3}He neutron spin filter (NSF) system developed at the China Spallation Neutron Source. The enclosed NSF cell, filled with ^{3}He at 2.53 bar, achieved an initial ^{3}He polarization of approximately 60%. After subsequent improvements in the magnetic field and heating system, this *in situ* system achieved a ^{3}He polarization of 75.66%± 0.09%, resulting in 96.30% neutron polarization at 2 Å. This highly compact *in situ* system is equipped with self-supportive features, pre-pumping capabilities, polarization maintenance, and a low-noise nuclear magnetic resonance system. These advantages significantly reduce the preparation time and simplify polarized neutron experiments, making it suitable for various neutron beamlines in China, particularly those with a limited sample space. These characteristics establish it as a quasi-standardized system that plays a vital role in polarized neutron experiments, including those involving polarized neutron imaging, neutron reflection, the performance calibration of polarized neutron instruments, and the neutron optics parity and time reversal experiment.

DOI: 10.1088/0256-307X/42/2/022901 CSTR: 32039.14.0256-307X.42.2.022901

1. Introduction. Polarized neutron technology plays a critical role in neutron-scattering experiments, particularly in advanced materials research.[1–4] Three primary methods are employed to obtain polarized neutrons: Heusler crystals,[5] polarizing supermirrors,[6] and polarized ^{3}He.[7] Compared with Heusler crystals and polarizing supermirrors, polarized ^{3}He has distinct advantages, including a large scattering angle, low background, broad energy spectrum, uniform polarization, and ability to flip neutron spins. Thus, polarized ^{3}He has been widely used in recent decades.[7,8]

Polarized ^{3}He is mainly produced through metastability-exchange optical pumping (MEOP)[9,10] or spin-exchange optical pumping (SEOP).[11,12] The SEOP method offers a compact size that can be easily incorporated into instruments. Moreover, the initial investment cost is almost one-tenth that of an MEOP system.[13] Furthermore, the *in situ* SEOP method can continuously polarize the neutron spin filter (NSF), and thus does not require decay calibration or a daily shift. Our previous work involved the development of an *off situ* ^{3}He NSF[14] and a first-generation *in situ* ^{3}He system (*in situ* 1) at the China Spallation Neutron Source (CSNS),[15] which made it possible to supply NSFs to some neutron beamlines. However, these suffered from the slow decay of the ^{3}He polarization[16] or a large size, which limited their utility in spectrometers with restricted space. To address the decay and size limitations, we developed a compact *in situ* NSF system. The volume of this new system has been significantly reduced (by nearly 1/2), which reduces the load on the beamline support and allows it to fit into tight spaces for sample analysis in neutron experiments. Moreover, the ^{3}He polarization of the new system reached 75.66% ± 0.09%, based on neutron measurements, making it a powerful and versatile tool for neutron scattering experiments. The development and commissioning of this compact *in situ* ^{3}He system are described in detail in this paper.

2. COMPACT in situ System. The primary challenge in constructing a more compact *in situ* NSF system is minimizing its length along the neutron pathway. Therefore, the guide field, magnet, and optical parts along the beam path must be optimized to release sufficient space and meet the space requirements of a spectrometer. The new *in situ* system was designed to be 55 cm wide (along the neutron beam path), 56 cm long, and 48 cm high, with

†These authors contributed equally to this work.
*Corresponding author. Email: zhangjunpei@ihep.ac.cn; tongxin@ihep.ac.cn
© 2025 Chinese Physical Society and IOP Publishing Ltd. All rights, including for text and data mining, AI training, and similar technologies, are reserved.

an overall weight of less than 50 kg. The system is self-supported and equipped with a height-adjustable function. The self-supporting cart was designed with a table size of 70 cm × 63 cm and weight of less than 200 kg. The height can be adjusted between 143 cm and 230 cm. This structure helps the system accommodate the neutron beam heights of different spectrometers. The mechanical design is illustrated schematically in Fig. 1. As shown in Fig. 1(a), the *in situ* NSF system employs four fans to facilitate heat exchange and ensure stable internal temperatures. The laser, heating, magnetic field, NSF, and optical systems are integrated inside the box. As seen in Fig. 1(b), the support equipment is stored within the frame, including function generator (Func Gen), data acquisition (DAQ), system control (Sys-Control), magnet driver (Mag-Driver), uninterrupted power supply (UPS), chiller, computer, and other slave equipment. The parameters of the *in situ* system are subsequently provided in detail.

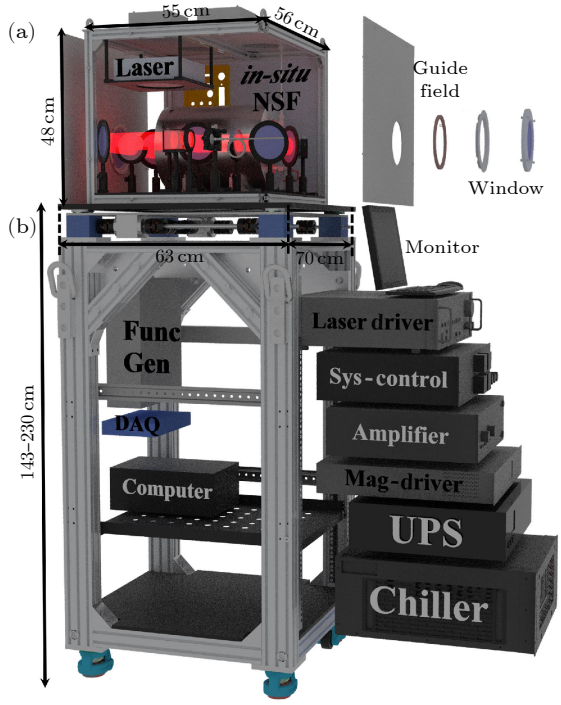

Fig. 1. Schematic of the compact *in situ* system. The optical setup can be found in Ref. [15]. (a) NSF part. (b) Supporting parts (Func Gen: function generator, DAQ: data acquisition, Sys-Control: system control, Mag-Driver: magnet driver, UPS: uninterrupted power supply).

Magnetic System. The magnetic field system is crucial for the polarization of ^{3}He.[11] Because of size limitations, the priority was to reduce the size of the magnet system to develop a compact *in situ* NSF system. The solenoid was designed to comprise 266 turns with a diameter of 25.5 cm and length of 33.2 cm. This was compensated for by two pairs of coils consisting of 5 turns and 18 turns. These coils were wound with copper wire ($\phi = 1$ mm), and their driving currents could be adjusted individually to ensure magnetic field uniformity. Additionally, a 2 mm thick μ metal layer was used to shield the stray field and provide a robust magnetic field for the SEOP process. Simulation results for the magnetic field were obtained using the finite element analysis software COMSOL[17] and are shown in Fig. 2. The magnetic field distributions in the solenoid and NSF are shown in Figs. 2(a) and 2(b), respectively. The volume-averaged transverse gradient of the NSF was 1.74×10^{-4}/cm [Fig. 2(c)].

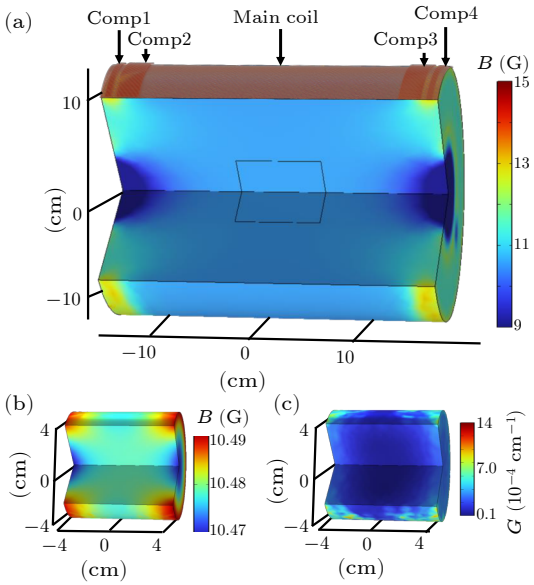

Fig. 2. (a) Simulated magnetic field in the solenoid. (b) Simulated magnetic field in the NSF region with the geomagnetic field environment. (c) Simulated magnetic field standardized transverse gradient of the NSF.

During the optimization of the magnetic field, a correlation between magnetic field gradient relaxation time $T_1^{\rm fg}$ ($\propto \frac{1}{|\vec{\nabla}B_x|^2+|\vec{\nabla}B_y|^2}$, $\frac{1}{T_1} = \frac{1}{T_1^{\rm fg}} + \frac{1}{T_{\rm wall}} + \frac{1}{T_{\rm dipole}}$) and relaxation time T_2 ($\propto \frac{1}{|\vec{\nabla}B_z|^2}$) of the free induction decay (FID) signal[18,19] was derived, as shown in Eq. (1). Here, the deduction of the correlation is based mainly on the current, where positive constant b depends only on the shape, pressure, and temperature of the NSF.[18] $\vec{\nabla}B_x$, $\vec{\nabla}B_y$, and $\vec{\nabla}B_z$ are the magnetic field gradients at the location of the NSF.[18,19] In addition, $\xi(a, x, y, z)$ is a positive constant function that depends only on the radius, (a), of the compensation coils and position, (x, y, z), of the FID coil. The detailed derivation can be found in Ref. [20]. Therefore, the magnetic field can be addressed using a fine-tuned current by monitoring the transverse relaxation time, T_2, signals of the two FID coils. After improving relaxation time T_2 from 12 ms to a maximum of 18 ms, combined with the actions of the other subsystems, the ^{3}He polarization increased from 60.09% to 68.70%, according to electron paramagnetic resonance (EPR) measurements.[16,21]

$$\frac{T_2}{T_1^{\rm fg}} = b \times \frac{|\vec{\nabla}B_x|^2 + |\vec{\nabla}B_y|^2}{|\vec{\nabla}B_z|^2} = b \times \xi(a, x, y, z). \quad (1)$$

Heating and laser system. In a typical SEOP process,[11] the ^{3}He NSF cell needs to be heated to approximately 200 ℃ to generate sufficient alkali metal vapor. Based on previous studies, a temperature distribution was generated in the NSF.[22] To improve the per-

formance of the heating system, an oven was optimally designed through thermal simulation using the finite element analysis software ANSYS,[23] which provided a uniform heating condition for the NSF, as shown in Fig. 3(a). Compared with the *in situ* 1 system,[15] the volume of the oven for the new compact system was reduced by 70%, as shown in Fig. 3(b). The control process for the heating system is illustrated in Fig. 4(a). A fuzzy proportional integral derivative (PID) algorithm was adopted to control the oven temperature. After carefully adjusting the parameters of the fuzzy PID algorithm, the precision of the heating system temperature control significantly improved. Additionally, the silicon dioxide thermal insulation layer (≈ 1 cm thick), which had a thermal conductivity of 0.017 W/(m·K), effectively reduced the pressure on the heat dissipation and μ metal shielding. The oven could then be heated to 195 ℃ within 0.5 h, with a temperature accuracy of ±0.15 ℃. The actual temperature data for the NSF surface during heating are shown in Fig. 4(b).

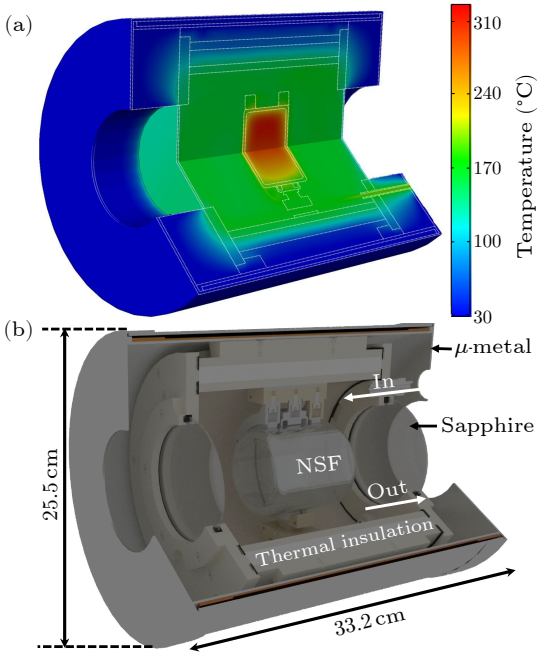

Fig. 3. (a) Simulated temperature distribution inside the oven. (b) Interior geometry of the oven.

The optical setup of this compact system was similar to that of the previous system,[15] with the lens, polarizing beam splitter, high laser reflecting and neutron transparent mirror, and quarter-wave plate positioned in the pumping path. A narrow line width (0.2 nm) high-power pumping laser delivering a total power of 160 W was employed to provide circularly polarized light to polarize the alkali atom. A pair of antireflective-coated sapphire windows was used to enhance the penetration of the pump laser, which also preserved the heat and neutron transmission. Additionally, a corresponding interlock system was installed to ensure the safe operation of the laser and heating system.

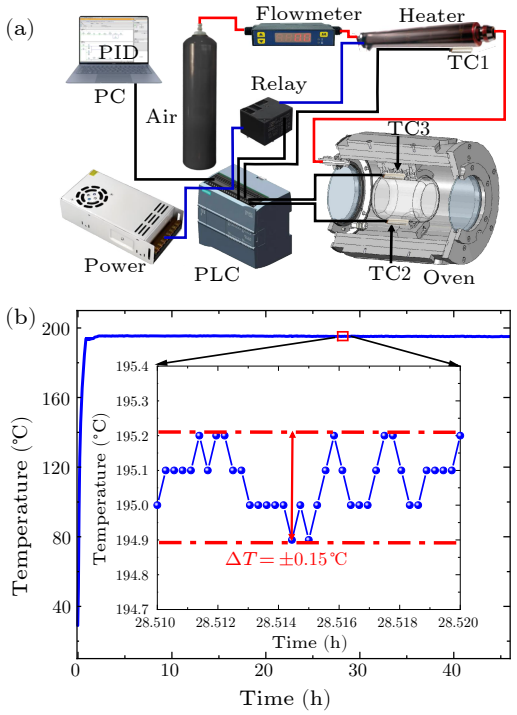

Fig. 4. (a) Control process for the heating system. (b) Actual temperature measured on the NSF surface.

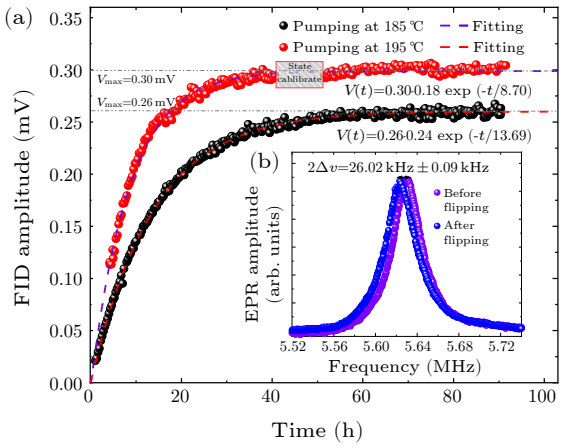

Fig. 5. (a) FID signal amplitude during the pumping process under 185 ℃ and 195 ℃. (b) Schematic of the EPR signal, with a frequency shift of $2\Delta v = 26.02 \pm 0.09$ kHz.

NSF. The installed cylindrical ^{3}He NSF, made of GE180, was produced in the filling station at CSNS.[24] It had an outer diameter of 8.0 cm, outer length of 8.0 cm, and wall thickness of 0.4 cm, resulting in an actual neutron path length of 7.2 cm for ^{3}He. The ^{3}He pressure was calibrated to 2.53 bar at 25 ℃ by neutrons at the BL-20 CSNS using the same method as in a previous study.[14]

Nuclear Magnetic Resonance (NMR) System. The NMR system incorporated FID technology,[16] EPR technology,[16,21] and Adiabatic Fast Passage (AFP) technology.[25,26] The FID technology was primarily used to monitor the state of the polarized ^{3}He. After carefully insulating the ground and filtering the power supply, the signal-to-noise ratio (SNR) of the FID signal reached a value of 25 upon saturation. The pumping data indicated that the spin-up time constants were 13.69 h at 185 ℃ and

8.70 h at 195 ℃. There was an obvious increase in the FID signal after the temperature increase, as shown in Fig. 5(a). The combination of the EPR and AFP technologies enabled the precise measurement of the absolute ^{3}He polarization. The measured AFP flipping loss was 0.3% per flip during the experiment. Additionally, an EPR frequency shift of 26.02 kHz ± 0.09 kHz was measured at 195 ℃, as shown in Fig. 5(b), which indicated a ^{3}He polarization of 77.48% ± 0.25%.

3. Commissioning on the Neutron Beamline. The *in situ* NSF system was calibrated on BL-20 with neutrons of 1.2–5.2 Å at the CSNS, as shown in Fig. 6. The polarization of ^{3}He, denoted by $P_{^3\mathrm{He}}$, could be derived from neutron transmission T_n through ^{3}He NSF as follows:[24]

$$T_\mathrm{n} = T_\mathrm{e}\exp(-n\sigma l)\cosh(n\sigma l P_{^3\mathrm{He}}). \tag{2}$$

T_0 is the neutron transmission for fully depolarized ^{3}He. According to Eq. (2), the fitted ^{3}He polarization was 75.66% ± 0.09%, as shown in Fig. 7.

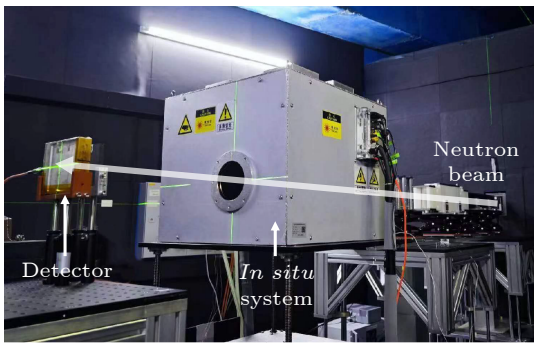

Fig. 6. Installation of the *in situ* system on BL-20.

The figure of merit (FOM) of the ^{3}He NSF is defined as $Q = P_\mathrm{n}^2 T_\mathrm{n}$, where $P_\mathrm{n} = \tanh(n\sigma l P_{^3\mathrm{He}})$ is the neutron polarization and T_n is the neutron transmission.[16] As shown in Fig. 8, the neutron polarization achieved a value of 96.30% at 2.0 Å, whereas Q attained a peak value of 0.226 at 1.50 Å.

The performance parameters of the *in situ* polarized ^{3}He systems used by different neutron sources are listed in Table 1. This shows that the performance of this *in situ* system reached an advanced international level.

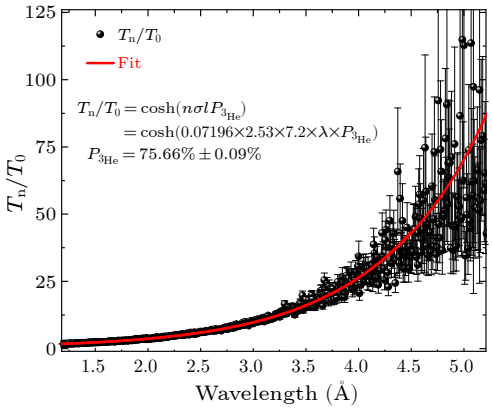

Fig. 7. Fitting of ^{3}He polarization at 1.2–5.2 Å wavelength.

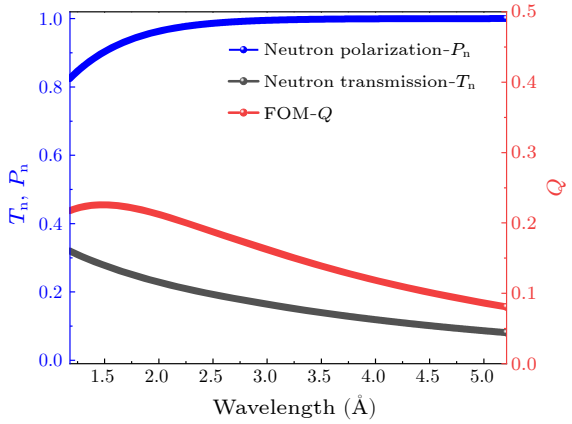

Fig. 8. Performance of the *in situ* NSF system as a function of the neutron wavelength. $T_\mathrm{e} = 0.85$ is assumed for all calculations in this paper.

Table 1. Performance parameters of some existing *in situ* polarized ^{3}He systems.

In-situ system	China, CSNS (this system)	China, CSNS[15]	UK, ISIS[27]	Germany, MLZ[28]	USA, SNS[29]	USA, HFIR[12]	Japan, J-PARC[13,30]
$P_{^3\mathrm{He}}$	75.56%	74.40%	63.00%	78.50%	84.00%	55.00%	73.00%
P_n	83.03%	64.54%	62.40%	99.38%	83.42%	81.46%	78.79%
p (bar)	2.53	1.58	1.69	3.00	2.30	3.00	3.76
V (cm^3)	55 × 56 × 48	70 × 70 × 60	85 × 65 × 45	62 × 20 × 40	69 × 59 × 54	30 × 66 × 44.5	60 × 60 × 30
d (cm)	8.0	7.2	11.0	5.0	7.0	5.8	3.4
l (cm)	8.0	8.7	8.8	15.0	8.0	8.8	5.3
L (cm)	55	70	85	62	69	30	60

$P_{^3\mathrm{He}}$: ^{3}He polarization, P_n: neutron polarization at 1.2 Å, p: NSF pressure, V: *in situ* system dimension, d: NSF diameter, l: NSF length, L: neutron pathway length of *in situ* system.

4. Conclusions. We successfully developed a new compact *in situ* NSF system. The new system meets the requirements of half the existing spectrometer space configurations and the ongoing construction of new neutron beamlines at the CSNS.

In addition, systematic modifications and optimizations were performed on the magnetic field, heat transfer, hosting system, and noise filtering to achieve the best ^{3}He polarization of 75.66% ± 0.09%, as measured by neutrons for a 2.53 bar ^{3}He NSF, enabling a 96.30% neutron polarization at 2 Å. The characteristics of this *in situ* system make it an ideal polarizer and analyzer for polarized neutron experiments. Currently, this *in situ* system has been employed at the CSNS in neutron experiments with a

multipurpose reflectometer (MR, CSNS[31]), test beamline (BL-20, CSNS), and back-streaming neutron line (Back-n, CSNS[32]), as well as for the cold neutron imaging beamline at the China Advanced Research Reactor (CNGC, CARR). Moving forward, we are committed to enhancing the performance of *in situ* systems to improve polarized-neutron applications.

Acknowledgements. This work was supported by the National Science Fund for Distinguished Young Scholars (Grant No. 12425512), the National Key Research and Development Program of China (Grant No. 2020YFA0406000), the National Natural Science Foundation of China (Grant No. 11875265), the Scientific Instrument Developing Project of the Chinese Academy of Sciences (Grant No. ZDKYYQ20190004), the Guangdong Basic and Applied Basic Research Foundation (Grant No. 2019B1515120079), Dongguan Introduction Program of Leading Innovative and Entrepreneurial Talents (Grant No. 20191122), and Guangdong Provincial Key Laboratory of Extreme Conditions, Dongguan Key Laboratory. We thank our glassblower Junsong Xie, who has supported this project since the beginning. We are grateful to Dr. Songlin Wang for his guidance during the neutron tests on BL-20 at the CSNS.

References

[1] Hang X D, Matsuda M, Held J T, Mkhoyan K A, and Wang J P 2020 *Phys. Rev. B* **102** 104402
[2] Krycka K, Borchers J, Ijiri Y, Booth R, and Majetich S 2012 *J. Appl. Crystallogr.* **45** 554
[3] Niketic N, van den Brandt B, Wenckebach W Th, Kohlbrecher J, and Hautle P 2015 *J. Appl. Crystallogr.* **48** 1514
[4] Petsch A N, Zhu M, Enderle M, Mao Z Q, Maeno Y, Mazin I I, and Hayden S M 2020 *Phys. Rev. Lett.* **125** 217004
[5] Ju J, Saito H, Kurumaji T, Hirschberger M, Kikkawa A, Taguchi Y, Arima T H, Tokura Y, and Nakajima T 2023 *Phys. Rev. B* **107** 024405
[6] Musgrave M M, Baeßler S, Balascuta S, Barrón-Palos L, Blyth D, Bowman J D, Chupp T E, Cianciolo V, Crawford C, Craycraft K, Fomin N, Fry J, Gericke M, Gillis R C, Grammer K, Greene G L, Hamblen J, Hayes C, Huffman P, Jiang C, Kucuker S, McCrea M, Mueller P E, Penttilä S I, Snow W M, Tang E, Tang Z, Tong X, and Wilburn W S 2018 *Nucl. Instrum. Methods Phys. Res. Sect. A* **895** 19
[7] Coulter K P, Chupp T E, McDonald A B, Bowman C D, Bowman J D, Szymanski J J, Yuan V, Cates G D, Benton D R, and Earle E D 1990 *Nucl. Instrum. Methods Phys. Res. Sect. A* **288** 463
[8] Tong X, Jiang C Y, Lauter V, Ambaye H, Brown D, Crow L, Gentile T R, Goyette R, Lee W T, Parizzi A, and Robertson J L 2012 *Rev. Sci. Instrum.* **83** 075101
[9] Andersen K H, Jullien D, Petoukhov A K, Mouveau P, Bordenave F, Thomas F, and Babcock E 2009 *Physica B* **404** 2652
[10] Wang Y T, Wu L Y, Zhang K Y, Peng M, Chen S Y, and Yan H Y 2024 *Sci. Chin. Phys. Mech. Astron.* **67** 273011
[11] Yan S, Zhang M F, Guo W C, Wang W Z, Gong J, Liang T J, Liu B Q, Peng M, Peng S M, Sun G A, Tu X Q, Yan H Y, Zhang J H, and Zheng H 2019 *Sci. Chin. Phys. Mech. Astron.* **62** 102021
[12] Jiang C Y, McDonald L, Cao H B, Balafas M, Crow L, and Kroll E 2023 *J. Phys.: Conf. Ser.* **2481** 012010
[13] Kira H, Sakaguchi Y, Oku T, Suzuki J, Nakamura M, Arai M, Endoh Y, Chang L J, Kakurai K, Arimoto Y, Ino T, Shimizu H M, Kamiyama T, Ohoyama K, Hiraka H, Tsutsumi K, and Yamada K 2011 *J. Phys.: Conf. Ser.* **294** 012014
[14] Huang C Y, Zhang J P, Ye F, Qin Z C, Amir S M, Buck Z N, Salman A, Kreuzpaintner W, Qi X, Wang T H, and Tong X 2021 *Chin. Phys. Lett.* **38** 092801
[15] Zhang J P, Huang C Y, Qin Z C, Ye F, Amir S M, Salman A, Dong Y C, Tian L, Buck Z N, Kreuzpaintner W, Musgrave M, Qi X, Wang T H, and Tong X 2022 *Sci. Chin. Phys. Mech. Astron.* **65** 241011
[16] Gentile T R, Nacher P J, Saam B, and Walker T G 2017 *Rev. Mod. Phys.* **89** 045004
[17] COMSOL Multiphysics 2023 v6.0. COMSOL AB (Stockholm, Sweden)
[18] Cates G D, Schaefer S R, and Happer W 1988 *Phys. Rev. A* **37** 2877
[19] McIver J W, Erwin R, Chen W C, and Gentile T R 2009 *Rev. Sci. Instrum.* **80** 063905
[20] Guo S H 2008 *Electrodynamics* (3rd ed.) (Beijing: Higher Education Press) p. 80 (in Chinese)
[21] Chann B, Babcock E, Anderson L W and Walker T G 2002 *Phys. Rev. A* **66** 032703
[22] Wang B, Zhang J P, Lu Y P, Huang C Y, Wang T H, Qin Z C, Dong Y C, Zheng Y J, Li J, Zhang W Q, Ye F, Qi X, Liu Y T and Tong X 2023 *J. Appl. Phys.* **133** 173105
[23] Ansys Inc. 2011 *Ansys Fluent Theory Guide* (USA)
[24] Qin Z C, Huang C Y, Buck Z N, Kreuzpaintner W, Amir S M, Salman A, Ye F, Zhang J P, Jiang C Y, Wang T H, and Tong X 2021 *Chin. Phys. Lett.* **38** 052801
[25] McKetterick T J, Boag S, Stewart J R, Frost C D, Skoda M W A, Parnell S R, and Babcock E 2010 *Physica B* **406** 2436
[26] Ino T 2018 *Proceedings of the International Conference on Neutron Optics* p. 011016
[27] Boag S, Babcock E, Andersen K H, Becker M, Charlton T R, Chen W C, Dalgliesh R M, Elmore S D, Frost C D, Gentile T R, Lopez Anton R, Parnell S R, Petoukhov A K, Skoda M W A, and Soldner T 2009 *Physica B* **404** 2659
[28] Salhi Z, Babcock E, Bingöl K, Bussmann K, Kammerling H, Ossovyi V, Heynen A, Deng H, Hutanu V, Masalovich S, Voigt J, and Ioffe A 2019 *J. Phys.: Conf. Ser.* **1316** 012009
[29] Jiang C Y, Tong X, Brown D R, Chi S, Christianson A D, Kadron B J, Robertson J L, and Winn B L 2014 *Rev. Sci. Instrum.* **85** 075112
[30] Jiang C Y 2023 *AAPPS Bulletin* **33** 21
[31] Zhu T, Zhan X Z, Xiao S W, Sun Y, Wu Y Y, Zhou A Y, and Han Q F 2018 *Neutron News* **29** 11
[32] Zhang M F, Yang Z, Zhang J P, Huang C Y, Wang T H, Chen Y H, Fan R R, Snow W M, and Tong X 2024 *Nucl. Instrum. Methods Phys. Res. Sect. A* **1072** 170184